Applied Thermal Engineering 195 (2021) 117203

Contents lists available at ScienceDirect

Applied Thermal Engineering

journal homepage: www.elsevier.com/locate/apthermeng

Performance of a horizontal heat exchanger for ground heat pump system: Effects of groundwater level drop with soil–water thermal characteristics

Ba Huu Dinh [a], Gyu-Hyun Go [b], Young-Sang Kim [c,*]

[a] Department of Architecture and Civil Engineering, Chonnam National University, Yongbong-ro 77, Buk-gu, Gwangju 61186, South Korea
[b] Department of Civil Engineering, Kumoh National Institute of Technology, Global 211, 61 Daehak-ro, Gumi, Gyeong-Buk 39177, South Korea
[c] Department of Civil Engineering, Chonnam National University, Yongbong-ro 77, Buk-gu, Gwangju 61186, South Korea

ARTICLE INFO

Keywords:
Groundwater table level drop
Thermal conductivity
Controlled low-strength material
Soil–water-thermal characteristic
Horizontal ground heat pump system

ABSTRACT

Horizontal Ground Heat Exchangers (HGHEs) are generally embedded at a shallow depth above the Ground-Water Table (GWT), where unsaturated soil exists. The change in the GWT strongly affects the thermal properties of the soil, and therefore influences the heat transfer efficiency of the HGHEs. This study evaluated the heat transfer performances of HGHEs with different backfill materials by considering the level drop of the GWT. In the experimental study, the soil–water characteristic curves and unsaturated thermal properties of backfill materials (natural sand, weathered granite soil, and controlled low-strength materials) were defined using modified 150-SWCC devices and a water extractor, coupled with a thermal conductivity measurement system. Subsequently, the influence of the GWT level change on the moisture content of the backfill materials was investigated using a seepage analysis (SEEP/W). Furthermore, finite element analyses were conducted to examine the influence of GWT level change on the thermal performances of the HGHEs. Based on thermal conductivity values experimentally obtained with corresponding volumetric water contents, the results from the experimental study indicate that thermal conductivity and volumetric water content have a linear relationship for all of the considered backfill materials. The results from the heat exchanger performance suggest that a HGHE backfilled with natural sand is the most affected by the GWT level drop among the three backfill materials, as it has the lowest air entry value and high-water content. In contrast, the HGHE backfilled with a controlled low-strength material is the least affected by the GWT level drop owing to its high air entry value and lowest water content. It is concluded a decrease in GWT level has a significant negative effect on the performances of HGHEs, especially when the decrease in the GWT level results in an increase in the soil suction that exceeds the air entry value of the backfill material.

1. Introduction

Among the various sources of renewable energy, geothermal energy is one of the most efficient and environmentally friendly [1]. Recently, studies on Ground Source Heat Pump (GSHP) systems have received increased attention, as they are expected to replace conventional cooling and heating systems and reduce greenhouse emissions [2]. According to American Environmental Protection Agency [3], using GSHP system can reduce the CO_2 emission from 15% to 77% compared to that of the fossil fuel heating system. In addition, the coefficient of performance of the GSHP system was significantly higher than that of the air source heat pump (i.e., 36%-38% for heating mode, and 32.0%-54.1% for cooling mode [4]). More recently, in 2020, a performance evaluation of the geothermal system with the different worldwide climatic zones indicated that using the earth to air heat exchanger can reduce up to 65% the cooling and heating capacity of the air handling unit (which is used to pre-treat the air in the traditional cooling and heating system) [5].

Depending on the installation orientation, a heat exchanger of the GSHP system can be divided into two groups: Vertical Ground Heat Exchanger (VGHE) or Horizontal Ground Heat Exchanger (HGHE). The VGHE approach is more widely used, because it is highly energy efficient and requires a smaller area [6,7]. However, an inevitable disadvantage of this system is its high construction cost (i.e., drilling operation cost) [8,9]. Because the excavation cost is much cheaper than the drilling cost, the HGHE is a good alternative to the VGHE. However, the heat transfer performance of the HGHE is not stable, and strongly depends on external factors such as evaporation from soils in the dry season, infiltration in

* Corresponding author.
E-mail address: geoyskim@jnu.ac.kr (Y.-S. Kim).

https://doi.org/10.1016/j.applthermaleng.2021.117203
Received 10 February 2021; Received in revised form 1 June 2021; Accepted 3 June 2021
Available online 11 June 2021
1359-4311/

Nomenclature

Symbols

A_p	pipe cross-sectional area (m^2)
C_p	specific heat capacity (J kg^{-1} K^{-1})
d_h	mean hydraulic diameter (m)
e_s	surface roughness
f_D	coefficient of friction
H	pressure head (m)
h	heat transfer coefficient of pipe wall (W m^{-2} K^{-1})
k	hydraulic conductivity (m s^{-1})
m_w	slope of the storage curve
n	porosity
Q	internal heat generation (W m^{-3})
Q_{wall}	external heat exchange between the pipe wall and surroundings (W m^{-3})
q	applied boundary flux (m^3 s^{-1})
Re	Reynolds number
r_0,r_N	inner, outer radii of the pipe wall, respectively (m)
r_n	outer radius of the n^{th} wall (m)
T	temperature (K)
T_f	fluid temperature (K)
T_p	external temperature of the pipe wall (K)
t	time (s)
u	fluid velocity (m s^{-1})
Z	wetted perimeter of the pipe (m)

Greeks

γ_w	unit weight of water (kg m^{-3})
θ_s	saturated volumetric water content
θ_w	volumetric water content
λ	thermal conductivity (W m^{-1} K^{-1})
λ_n	thermal conductivity of the n^{th} wall (W m^{-1} K^{-1})
ρ	density (kg m^{-3})
χ	volumetric fraction
ψ	matric suction (kPa)
ψ_r	residual matric suction (kPa)

Abbreviations

CLSM	controlled low-strength material
GHE	ground heat exchanger
GSHP	ground source heat pump
GWT	groundwater table
HGHE	horizontal ground heat exchanger
NS	natural sand
SWCC	soil–water characteristic curve
VGHE	vertical ground heat exchanger
WGS	weathered granite soil

Subscripts

ext, int	external, internal, respectively
f	fluid
p	pipe
s, w, a	solid, water, and air, respectively

the rainy season, and atmosphere-soil interactions [9,10]. Many studies have been conducted to evaluate the performances of HGHEs in different conditions. Cogedo et al. [11] examined the key factors influencing the heat transfer efficiency of horizontal GHPSs using a numerical analysis. They found that the high thermal conductivity of the ground (3 W m^{-1} K^{-1}) resulted in approximately double the thermal performance of GHE relative to that at a low ground thermal conductivity (1 W m^{-1} K^{-1}). Go et al. [9] evaluated the performance of an HGHEs by considering the effects of infiltration and groundwater advection. The results indicated that infiltration had a positive effect on the heat performance of the system and caused an increase in the difference between the outlet and inlet temperatures of the circulating fluid. Gan [12] developed a model for considering the impact of coupled heat and moisture transfers on the dynamic thermal performance of an HGHE. It was found that the heat transfer through an HGHE with consideration of moisture transfer was up to 24% lower than without consideration of moisture transfer. More recently, Tang and Nowamooz [10] investigated the effects of atmosphere-soil interactions on the outlet temperature of a slinky HGHE. The results showed that the avoiding consideration of the atmosphere-soil interaction overestimated the fluid outlet temperature by approximately 17% at the installation depth, ranging between 0.5 and 2 m and 48% for an installation depth between 0.5 and 1 m.

The thermal conductivities of the surrounding soil and backfill material are strongly affected by its water content. Abu-Hamdeh and Reeder [13] used the thermal probe to measure the thermal conductivity of various soil types (loam, clay loam, sand, and sandy loam) at different water content. The result indicated that water content had a positive effect on the thermal conductivity of soil, regardless of the soil types. Xu et al. [14] evaluated the effect of water content and dry density on the thermal conductivity of silty clay. They concluded that the thermal conductivity decreased with the decrease in the water content and dry density, and water content has a higher influence on the thermal conductivity than the dry density. Allan and Kavanaugh [15] measured the thermal conductivity of net cementitious grouts at saturated and dry conditions. They found that the thermal conductivity of saturated grouts (with the water to cement ratio of 0.8) reduced approximately half after completely dried. Delaleux et al. [16] found that the thermal conductivity of bentonite grout used for geothermal borehole heat exchangers reduced 1 W/mK for a 10% decrease in water content.

Generally, HGHE is buried at the shallow depth (1–3 m) above the GWT, where the unsaturated soil exists [17]. Due to the influence of water content, the thermal conductivity of the unsaturated soil above the GWT is significantly lower than that under the saturated conditions below the GWT. Furthermore, the GWT fluctuates owing to many factors, such as climate change, atmospheric pressure, aquifer deformation, earthquakes, and human activities [18–20]. For instance, in Jeju island (South Korea), the annual GWT fluctuation varied between approximately 0.1 to 5 m (Fig. 1) [18]. Among the 57 groundwater level monitoring wells studied, 72.4% showed a decrease in the GWT. These decreases resulted from the rapidly increasing population and agricultural activities [18]. A change in the GWT may influence the unsaturated thermal properties of the soils located above the GWT, and hence affect the heat transfer efficiency of the HGHE system. Nevertheless, the effect of a GWT level drop on the performance of an HGHE has rarely been

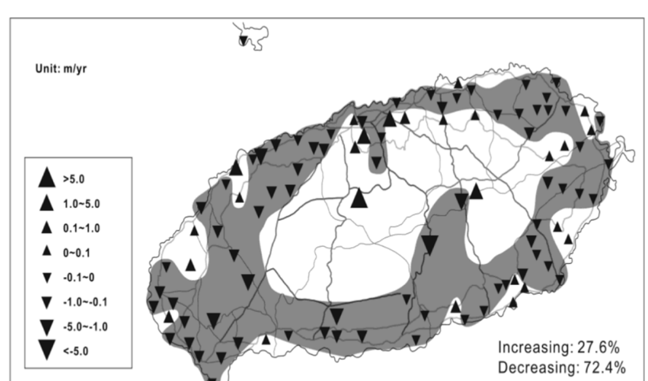

Fig. 1. Annual change in groundwater table in Jeju island [18].

evaluated.

Thus, this study investigated the performance of HGHEs with different backfill materials by considering the GWT level drop. For this purpose, the soil–water-thermal conductivity characteristics of the soils and backfill materials were obtained by combining the results from modified 150-Soil-Water Characteristic Curve (SWCC) devices and a high-pressure membrane extractor; this allowed for direct measurement of the thermal conductivity, under a wide moisture content range. Subsequently, a seepage analysis was conducted to model the changes in the degrees of saturation of the backfill materials caused by the GWT level drop. Finally, finite element analyses were conducted to examine how the GWT influenced the performances of the HGHEs considering the soil–water-thermal characteristics of the backfill materials.

2. Material and experimental program

2.1. Backfill materials

In general, excavated soil is used to backfill an HGHE system and acts as a heat transfer medium between the GHE and surrounding soils. In this study, Weathered Granite Soil (WGS), which is frequently used as a backfill material and in the surrounding soil of heat exchangers, was compared with other backfill materials such as Natural Sand (NS) and Controlled Low-Strength Materials (CLSMs). NS or silica sand containing SiO_2 has high thermal conductivity, whereas CLSMs have shown good performance in terms of workability and provide relatively high thermal conductivity; thus, they were considered as a potential heat transfer media for the HGHE [21,22]. The frequency of each grain size and other physical properties of the WGS and NS are displayed in Fig. 2, and Table 1, respectively.

Conventionally, CLSM was utilized for multiple purposes such as void fill, backfill, structural fill, pavement base [23]. A CLSM mixture typically contents a larger amount of fine aggregate (i.e., natural sand (1543–1833 kg m^{-3})), a small amount of cement (30–199 kg m^{-3}), fly ash (0 –1186 kg m^{-3}), by-product (297–564 kg m^{-3}), and water (193–593 kg m^{-3}) [23]. In this study, a by-product (steel slag) was used to replace the natural sand in the mixture. Steel slag containing free lime (CaO) and SiO_2 has a pozzolanic reaction with fly ash [22]; thus, both the mechanical and thermal properties of the mixture were improved. The void ratio decreased, the compressive strength increased, the thermal conductivity was enhanced [22]. Table 2 lists the proportions and engineering properties of the CLSM mixtures used in this study. The advantages of the CLSM include its self-leveling and self-compacting abilities, owing to its high workability [23,24]. Fresh CLSM can backfill voids without any compaction effort. According to ACI 299-R [23], engineering properties of the CLSM required for general backfill purposes are: (1) flowability higher than 20 cm, (2) bleeding lower than 5%, (3) setting time no later than 36 h, (4) unconfined compressive strength ranging from 0.3 to 8.3 MPa. As shown in Table 2, the CLSM mixture used in this study satisfied all engineering properties for backfill purposes, i.e., the high flowability (21 cm), normal bleeding (2%), early setting time (10.5 h), and high compressive strength (3.5 MPa).

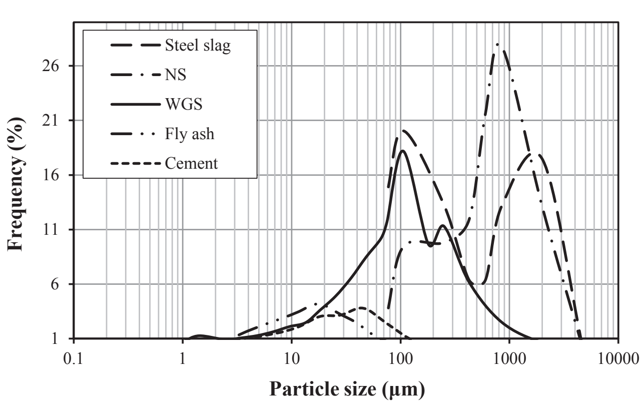

Fig. 2. Frequency of each grain size of weathered granite soil (WGS), natural sand (NS), and raw materials for controlled low-strength material (CLSM).

Table 1
Physical properties of soils and steel slag.

Description	Natural sand (NS)	Weathered granite soil (WGS)	Steel slag
Maximum dry density (kg m^{-3})	1780	1576	2280
Optimum Moisture Content OMC (%)	12.5	18.8	13.8
Specific gravity	2.65	2.62	3.39
Thermal conductivity (W m^{-1} K^{-1})	1.58	1.30	1.39

Table 2
Proportions and general properties of controlled low-strength material (CLSM) mixtures.

	Description	Value
Proportion	Sand (kg m^{-3})	896
	Steel slag (kg m^{-3})	441
	Fly ash (kg m^{-3})	320
	Cement (kg m^{-3})	113
	Water (kg m^{-3})	351
General properties	Flowability (cm)	21
	Bleeding (%)	2
	Initial setting time (h)	10.5
	Compressive strength (28 days) (MPa)	3.5

2.2. Soil-water characteristic curve (SWCC) and thermal properties of unsaturated backfills

HGHEs are generally constructed above the GWT. Accordingly, the backfill materials and soil surrounding the ground heat exchanger have unsaturated conditions. SWCCs, which represent the relationship between soil suction and volumetric water content, are well-known as the most important parameters for determining the properties and behavior of unsaturated soils [25]. A typical SWCC includes three zones: a boundary effect zone, transition zone, and residual zone [25]. The transition zone and boundary effect zone are separated by the Air Entry Value (AEV). At the AEV, the largest pore size occupied by water starts to detach from the soil. When the matric suction exceeds the AEV, the water in the soil is rapidly displaced by air, until it reaches the residual water content. Beyond the residual water content, as the matric suction decreases, the volumetric water content decreases very slowly, as the water in the soil is retained by the absorption force. The Fredlund and Xing model [25] for a full SWCC is expressed as follows:

$$\theta_w = C(\psi)\frac{\theta_s}{\{ln[e+(\psi/a)^n]\}^m} \tag{1}$$

$$C(\psi) = \frac{ln(1+\psi/\psi_r)}{ln(1+10^6/\psi_r)} \tag{2}$$

In the above, $m, n,$ and a are fitting parameters, ψ (kPa) is the soil suction corresponding to the volumetric water content θ_w, $C(\psi)$ is a correction factor, $\psi_r$is the matric suction at the residual water content, $\theta_s$is the saturated volumetric water content, and the irrational constant, e, can be approximated as 2.71828 [25].

In this study, the SWCC curves for the NS and WGS were determined using SWCC −150 Fredlund SWCC devices. In the SWCC test for the CLSM mixtures, a high-pressure membrane extractor with a maximum pressure of 10 MPa was employed. In addition, to determine the relationships between the thermal conductivities and water contents of the backfill materials, both the SWCC device and high-pressure membrane extractor were modified by coupling them with a thermal measurement system. The thermal measurement system included a thermal needle connected to a DC supplier, ammeter, and data logger software. The thermal conductivity measurements were conducted according to the transient hot-wire method; the testing procedure has been reported in detail in previous studies [21,22]. The SWCC test devices and thermal conductivity measurement system are shown in Fig. 3 and Table 3.

2.3. Seepage analysis

A drop in the GWT level causes a decrease in the water pressure (increase in soil suction), resulting in a decrease in the volumetric water content of the soil. In this study, the commercial software SEEP/W was used for the seepage analysis of the changes in the GWT. The governing equation for the seepage is presented in Eq. (3).

$$m_w\gamma_w\frac{\partial H}{\partial t} = \nabla(k\nabla H) + q \quad (3)$$

Here, H is the pressure head (m), t is the time (s), γ_w is the unit weight of water (kg m^{-3}), m_w is the slope of the storage curve, q denotes the applied boundary flux (m^3 s^{-1}), and k is the hydraulic conductivity (m s^{-1}).

Fig. 4 shows the boundary conditions and geometry of the SEEP/W domain. A soil model domain with a height of 12 m and width of 30 m was constructed, with a mesh size of 0.25 m (rectangular grid). The heat exchanger was located at depths ranging from − 2 m to − 4 m, which was the general depth where the HGHEs were located. The GWT was assumed to be located at − 2 m depth; thus, initially, the backfill materials were saturated, and the soil from the ground surface to a depth of −2 m was considered as unsaturated soil.

To evaluate the effect of the GWT level drop on the unsaturated properties of the backfill materials, the GWT level was assumed to linearly drop from − 2 m to − 12 m over 300 days (decreasing 1 m for 30 days). Before conducting the seepage analysis, a steady-state analysis was conducted for 48 h to achieve the hydrostatic condition; thus, the pore pressure ranged from − 20 kPa at the ground surface to 0 kPa at GWT as the initial condition. Fig. 5 displays the grid independence and time-step independence results. The pore water pressure converged at the total of 5760 elements corresponding to the mesh-size of 0.25 m (Fig. 5(a)), and the number of time step of 480 (Fig. 5(b)); thus, to reduce the calculation time and the memory size of the model, the mesh size of 0.25 m and the number of time-step of 480 were opted. Note that the SWCC curves measured in Section 2.2 (Fig. 6) and their corresponding hydraulic conductivities (Fig. 7) were used as the input data for the SEEP/W model. These SWCCs were fully built using Fredlund and Xing's model; their fitting parameters are listed in Table 4.

Table 3
The devices used for the thermal conductivity measurement.

Devices	Description	Measurement range	Accuracy
DC supplier	Keysight E3620A	0 V to 25 V	±0.5%
Ammeter	Keysight 34461A	100 μA to 10 A	≤0.25%
Data logger	Keysight 34461A	100 Ω to 100 MΩ	≤0.81%
Thermal needle	Length 30 mm, diameter 1.27 mm	0 °C to 50 °C	≤5%

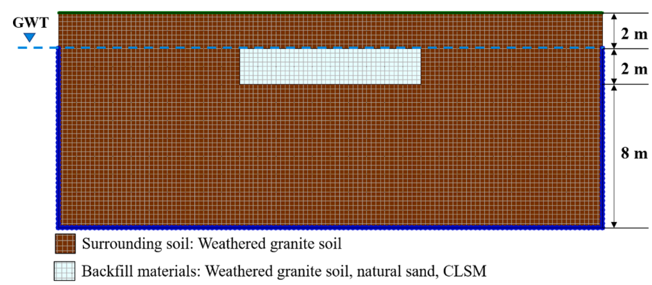

Fig. 4. SEEP/W model domain.

2.4. Thermal performance analysis

In this study, the thermal performance analysis of the HGHEs with different backfill materials was conducted using a commercial finite element code program (COMSOL Multiphysics). The heat transfer in the model includes the heat conduction inside the surrounding soil and backfill materials and the heat convection between the pipe wall and circulating water. Based on Fourier's law, the heat transfer in the solid of this model can be expressed as follows:

$$\rho C_P\frac{\partial T}{\partial t} + \nabla(-\lambda\nabla T) + Q = 0 \quad (4)$$

Furthermore, if the HGHEs are located above the GWT, the surrounding soil and backfill materials are defined as a porous medium comprising of three phases: air, water, and solid. Accordingly, the equivalent thermal conductivity of the porous medium can be expressed as follows:

$$\lambda = \sum_{j=1}^{3}\chi_j \times \lambda_j \ \ (j = air, water, solid) \quad (5)$$

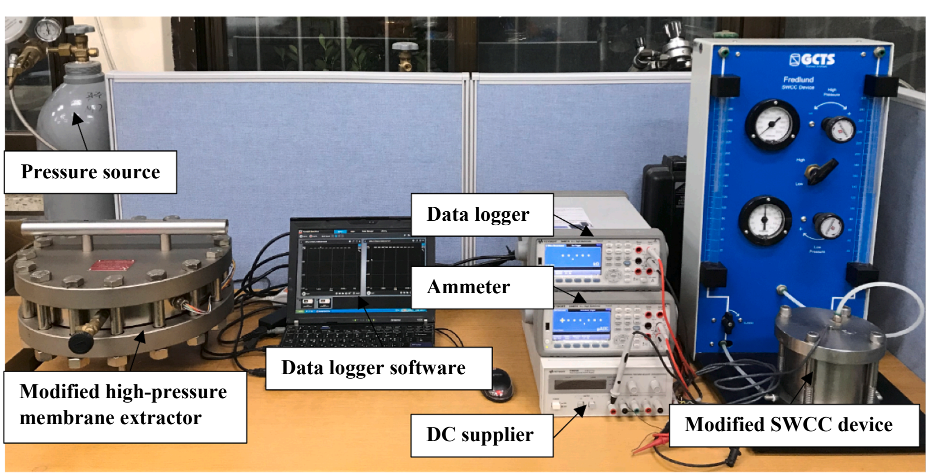

Fig. 3. Thermal conductivity test with SWCC devices.

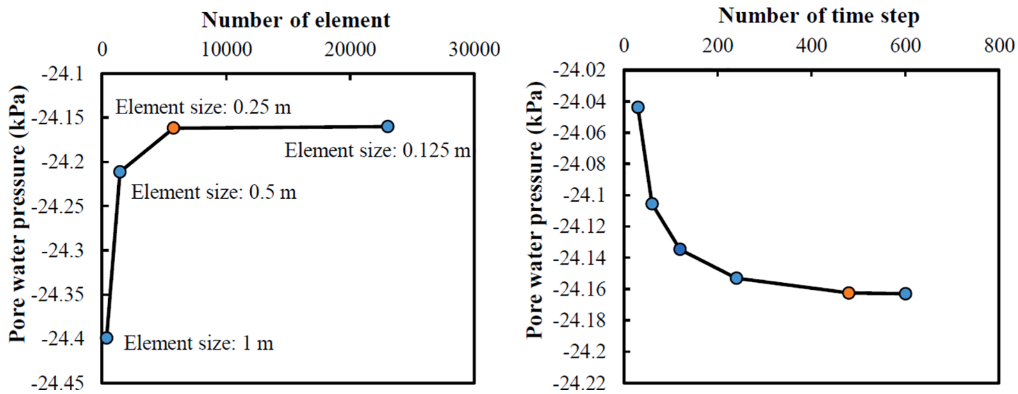

Fig. 5. (a) Grid independence results and (b) time step independence results for seepage analysis model (SEEP/W).

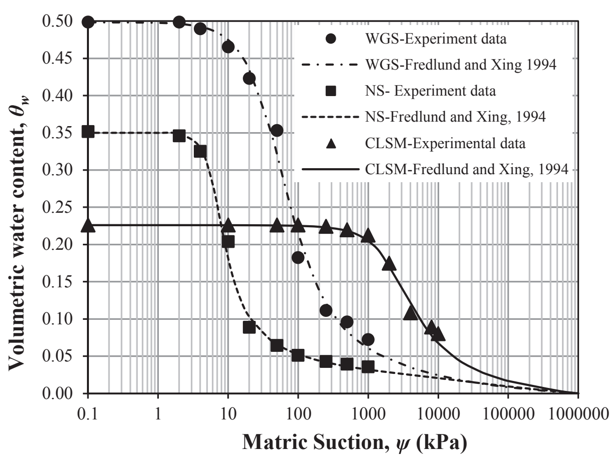

Fig. 6. SWCCs of different backfill materials for horizontal ground heat exchangers (HGHEs).

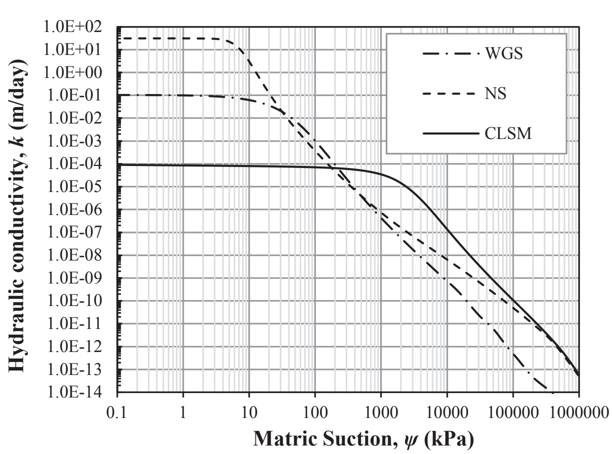

Fig. 7. Hydraulic conductivity- matric suction.

Table 4
Properties and fitting parameters for the soil–water characteristic curves (SWCCs) of soils and CLSM.

Materials	θ_s	K_s (m s^{-1})	a	n	m	AEV (kPa)
NS	0.35	10^{-4}	6	3.8	0.8	4
WGS	0.49	10^{-6}	44	1.6	1.3	16
CLSM	0.226	10^{-9}	2200	1.90	0.90	1000

$$\chi_{solid} = 1 - n \tag{6}$$

$$\chi_{water} = \theta_w \tag{7}$$

$$\chi_{air} = n - \theta_w \tag{8}$$

Here, λ_j represents the thermal conductivity of air, water, and solid phases; n is the porosity; χ_j denotes the volumetric fraction of each phase, which is calculated from Eq. (1).

The energy equation for the heat transfer of the fluid flow in a GHE pipe is expressed as follows:

$$\rho_f A_p C_p \frac{\partial T_f}{\partial t} + \rho_f A_p C_p u \cdot \nabla T_f = \nabla \cdot (\lambda_f A_p \nabla T_f) + \frac{1}{2} f_D \frac{\rho A_p}{2d_h} |u| u^2 + Q + Q_{wall} \tag{9}$$

In the above, $(1/2) f_D (\rho A_p / 2d_h) |u| u^2$ represents the friction heat dissipated owing to the viscosity of the fluid, where u is the tangential fluid velocity of the fluid (m s^{-1}), d_h indicates the mean hydraulic diameter (m), and f_D denotes the coefficient of friction calculated by Churchill's friction model (Eqs. (10), (11), (12)) [26].

$$f_D = 8\left[\left(\frac{8}{Re}\right)^{12} + (C_A + C_B)^{-1.5}\right]^{1/12} \tag{10}$$

$$C_A = \left[-2.457 ln\left(\left(\frac{7}{Re}\right)^{0.9} + 0.27\left(\frac{e_s}{d_h}\right)\right)\right]^{16} \tag{11}$$

$$C_B = \left(\frac{37530}{Re}\right)^{16} \tag{12}$$

Furthermore, the external heat exchange between the pipe wall and surroundings, Q_{wall}, can be expressed as follows:

$$Q_{wall} = (hZ)_{eff}(T_p - T_f) \tag{13}$$

In the above, the effective hZ(W m^{-1} K^{-1}) for a circular tube can be obtained as follows:

$$(hZ)_{eff} = \frac{2\pi}{\frac{1}{r_0 h_{int}} + \frac{1}{r_N h_{ext}} + \sum_{n=1}^{N} \frac{ln\left(\frac{r_n}{r_{n-1}}\right)}{\lambda_n}} \tag{14}$$

In the above, $r_0$and $r_N$are the inner and outer radii of the pipe wall (m), respectively, and $r_n$represents the radius of the nth wall (m); thus,r_n ranges from $r_0$tor_N. In addition, $h_{ext}$and h_{int}indicate the film heat transfer coefficients outside and inside the pipe wall, respectively, and $\lambda_n$represents the thermal conductivity of the nth wall (W m^{-1} K^{-1}).

Fig. 8 presents a finite element model with dimensions of 10 × 30 × 12 m (width × length × depth) for the simulation of the heat transfer of

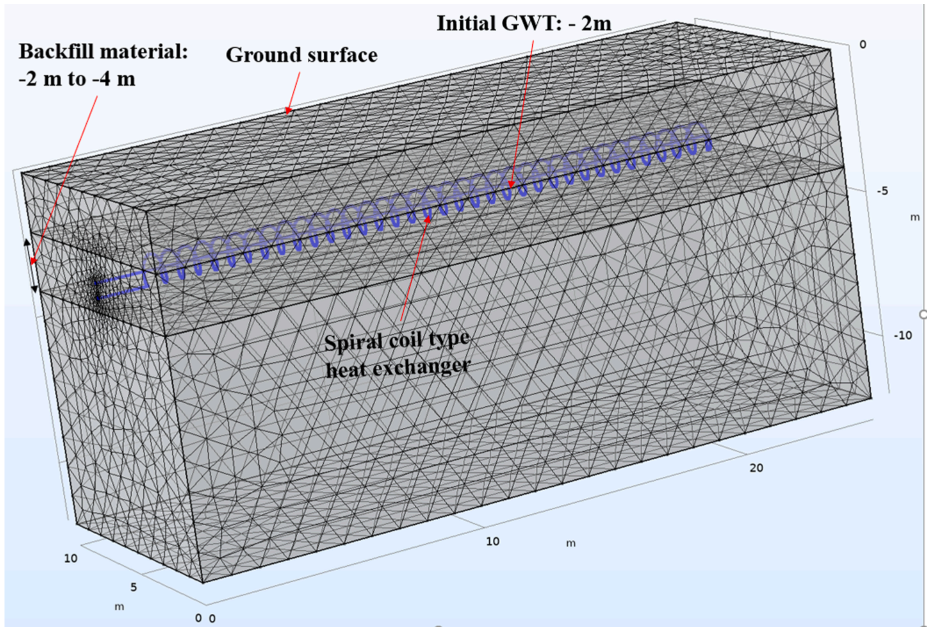

Fig. 8. Geometry for numerical analysis.

the HGHEs. In this study, a spiral coil was used as the GHE pipe, with extremely fine meshes. Fig. 9(a) displays the relationship between the outlet fluid temperature and the number of elements. The outlet fluid temperature converged at a fine mesh size with a total of 320,160 elements. Therefore, the backfill material and surrounding soil were modeled using a fine triangular mesh size with a maximum unit length of 1 m, so as reduce the calculation time. The flow rate and the inlet fluid temperature were assumed as constant as 2 l/min and 3 °C, respectively. Fig. 9(b) presents the time-step independence results. The outlet fluid temperature converged at the time-step of 0.01 h (a total of 816 steps); thus, this time-step value was used for the model. Regarding the GHE pipe, a spiral coil with a pitch of 30 cm, radius of 25 cm, and a total of 50 coil turns were located at a depth of −3 m, to minimize the surface effect [11]. The backfill material was located at a depth ranging from −2 to −4 m to match the geometry of the SEEP/W model. The general thermal properties of the materials used in the numerical analysis model are listed in Table 5. The saturated thermal properties of the backfill materials shown in Table 5 were measured using a KD2 thermal properties analyzer according to ASTM D 5334 [27]. It should be noted that the water content not only affected the thermal conductivity but also influenced the density and specific heat capacity of the materials [28]. Thus, the density and specific heat capacity of the unsaturated soils located above the GWT were calculated using Eq. (15) and Eq. (16), respectively.

Table 5
Input parameters for the numerical analysis model.

Material	Thermal conductivity (W m^{-1} K^{-1})	Specific heat capacity (J kg^{-1} K^{-1})	Density (kg m^{-3})
Polybutylene pipe	0.38	525	955
Circulating water	0.58	4180	1000
Saturated weathered granite soil	1.35	1615	2066
Saturated natural sand	1.59	1322	2130
Saturated CLSM	2.25	1213	2121
Unsaturated backfill materials	From SWCC	From SWCC	From SWCC

$$\rho = \chi_s\rho_s + \chi_w\rho_w + \chi_a\rho_a \tag{15}$$

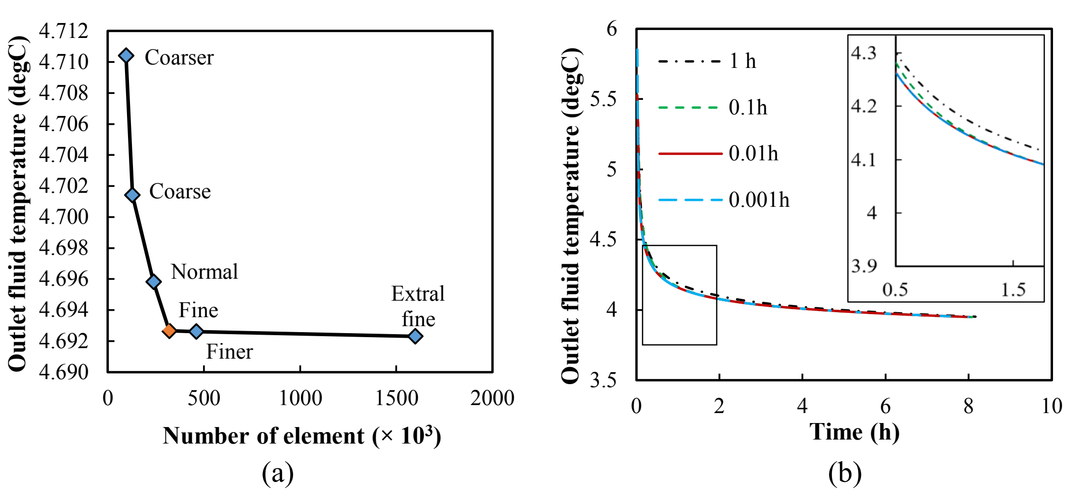

Fig. 9. (a) Grid independence results and (b) time step independence results for heat transfer model (COMSOL).

$$C = \frac{\chi_s \rho_s C_s + \chi_w \rho_w C_w + \chi_a \rho_a C_a}{\chi_s \rho_s + \chi_w \rho_w + \chi_a \rho_a} \quad (16)$$

Here, the subscripts *s, w,* and *a* represent the solid, water, and air phases, respectively; ρ is the density (kg m^{-3}); χ is volumetric fraction; and C denotes the specific heat capacity (J kg^{-1} K^{-1}). The air fraction is ignored owing to its low density (1.2 kg m^{-3} at 20 °C) [29]. The fractions of the solid and water phases under unsaturated conditions varying with depth were determined using the SWCC curves. The input databases of the finite element model for the heat exchange evaluations of the HGHEs at the initial GWT (- 2 m) are presented in Fig. 10.

3. Results and discussion

3.1. Thermal conductivity of backfill materials at saturation and completely dry conditions

The thermal conductivities of the WGS, NS, and CLSM at completely dry and saturated conditions varied from 0.37 to 1.36 W m^{-1} K^{-1}, 0.33 to 1.58 W m^{-1} K^{-1}, and 1.18 to 2.25 W m^{-1} K^{-1}, respectively (Fig. 11). Evidently, thermal conductivity of the CLSM is significantly higher than that of NS and WGS under both dry and saturated conditions. Furthermore, among the three backfill materials, the CLSM has the lowest difference in thermal conductivity between the saturated and dry conditions as shown in Fig. 11. This is attributed to the low volumetric water content of the CLSM. The thermal conductivity of water is 0.6 W m^{-1} K^{-1}, i.e., approximately 24 times higher than that of the air (0.025 W m^{-1} K^{-1}). Under dry conditions, the water in the soil is replaced by air, resulting in a decrease in the thermal conductivity. Therefore, owing to the high volumetric water content, the thermal conductivities of the WGS and NS at saturation and dry conditions are significantly different (72.8% and 71.9%, respectively). The results also demonstrate that the volumetric water content is an important factor affecting the thermal conductivity of the backfill materials.

3.2. Thermal conductivity of unsaturated backfill materials and thermally predicted models

The relationships between the thermal conductivity and volumetric water content of the backfill materials are shown in Fig. 12. A linear relationship is observed for the sand and CLSM. Regarding the WGS, as the volumetric water content decreases, the thermal conductivity remains almost constant, and then decreases afterward. Interestingly, the indicator for the volumetric water content value at the inception of the decrease in thermal conductivity is θ_{AEV} corresponding to the volumetric water content at the AEV. At saturation (suction equals zero), free

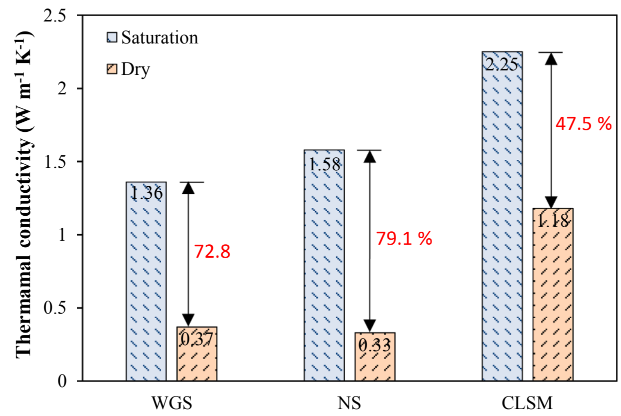

Fig. 11. Thermal conductivities of backfill materials in saturated and completely dry conditions.

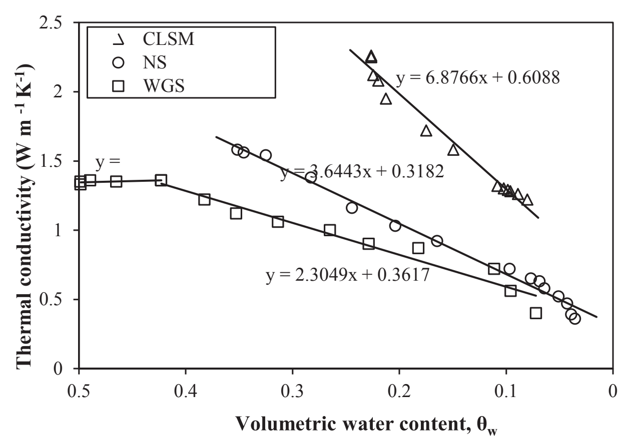

Fig. 12. Thermal conductivity and volumetric water content relationships.

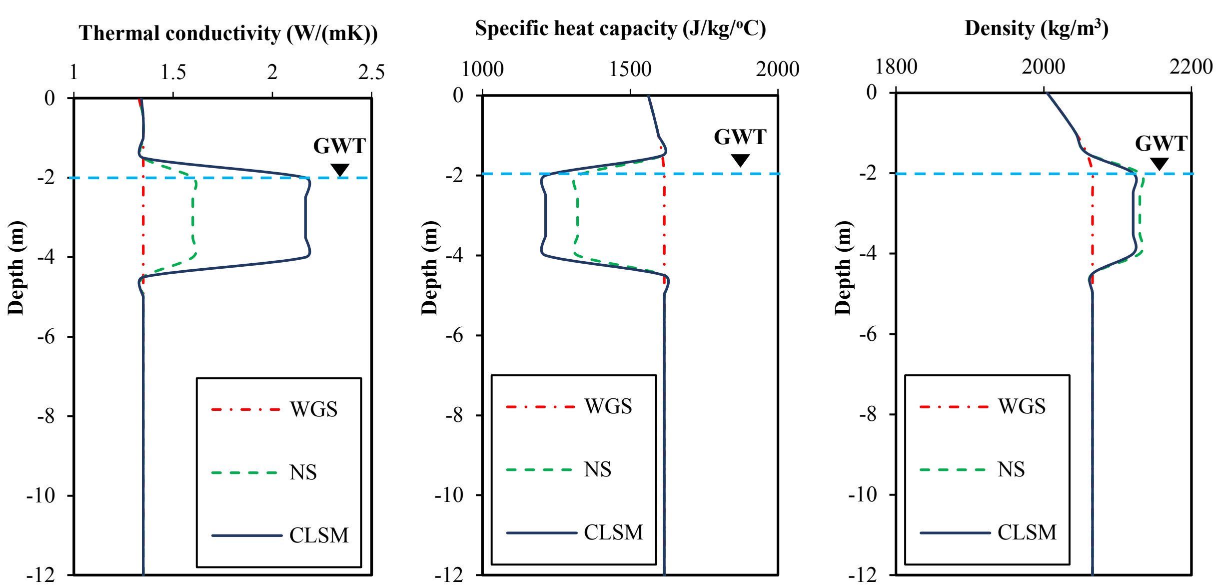

Fig. 10. Initial conditions for numerical analysis.

water fills the pores between the soil particles. Under suction below the AEV, the free water is gradually removed, but the air has not yet entered the pores; accordingly, the thermal conductivity remains constant. Previous studies [21,30] found that the thermal conductivity in this stage slightly increases with the decrease in volumetric water content owing to the decrease in free water leading to the soil particles coming closer. Consequently, the contact area between the thermal needle probe and soil increases resulting in an increase in the soil thermal conductivity [30]. Under suction beyond the AEV, the air starts to replace the water in the pores; thus, the thermal conductivity of the soil is reduced.

The thermal conductivities of the backfill materials vary from λ_s (saturated thermal conductivity) to λ_d (completely dry thermal conductivity). To build the thermal conductivity prediction model, a normalized analysis was conducted using the thermal conductivity measurement results presented in Fig. 11 and Fig. 12. The relationship between the normalized thermal conductivity and volumetric water content ($(\lambda - \lambda_d)/(\lambda_s - \lambda_d)$ vs. θ_w) and the predictive models for thermal conductivity estimations of the NS, WGS, and CLSM are presented in Fig. 13 and Table 6, respectively.

3.3. Effect of GWT level drop on thermal conductivity of backfill materials

Fig. 14 presents the thermal conductivity variations in the unsaturated WGS caused by the GWT level drop. The pore water pressure versus depth, as a result of the SEEP/W analysis, is displayed in Fig. 14 (a). When the GWT level drops, the pore water pressure decreases, leading to an increase in the suction and a decrease in the volumetric water content. In this case, the SWCC from the experimental results (Fig. 6), which provides the relationship between the matric suction and volumetric water content, can be used to convert the pore water pressure versus depth (Fig. 14(a)) to a volumetric water content versus depth (Fig. 14(b)). To determine the thermal conductivity profile (Fig. 14(c)), the empirical models in Table 6 are employed. The variables for the empirical models are the thermal conductivity at saturated and completely dried conditions (λ_s and λ_d) as depicted in Fig. 11, the volumetric water content (θ_w) denoted in Fig. 14(b), and the volumetric water content at the AEV (θ_{AEV}), i.e., from the SWCC curve presented in Fig. 6. Using the same analysis method presented above, the thermal conductivity profiles of the NS and CLSM are shown in Fig. 15(c) and Fig. 16(c), respectively.

Notably, backfill materials (WGS, NS, CLSM) exist at depths between −2 m and −4 m, where the GHE is located, whereas the surrounding soil (WGS) exists at depths between 0 m to −2 m and −4 m to −12 m. When the GWT decreases from −2 m to −12 m, the thermal conductivities of the WGS and NS at the middle of GHE (depth = -3 m) are significantly

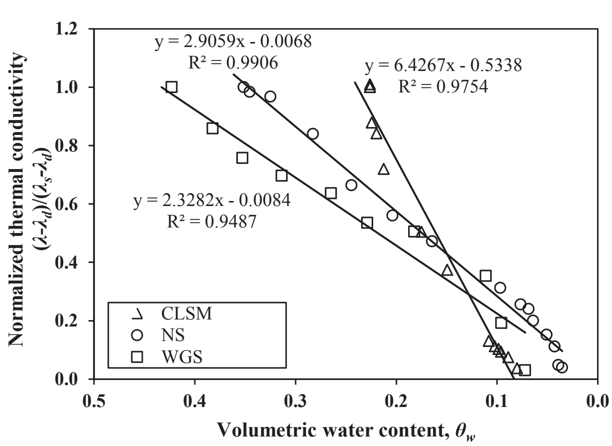

Fig. 13. Relationship between normalized thermal conductivity and volumetric water content.

Table 6
Predictive models for thermal conductivity of NS, WGS and CLSM.

Materials	Predictive models	R^2
NS	$\lambda = (\lambda_s - \lambda_d) \times (2.9059 \times \theta_w - 0.0068) + \lambda_d$	0.9906
WGS	$\lambda = \lambda_s$ when $\theta_s \geq \theta_w \geq \theta_{AEV}$	0.9487
	$\lambda = (\lambda_s - \lambda_d) \times (2.3282 \times \theta_w - 0.0084) + \lambda_d$ when $\theta_w \leq \theta_{AEV}$	
CLSM	$\lambda = (\lambda_s - \lambda_d) \times (6.4267 \times \theta_w - 0.5338) + \lambda_d$	0.9754

*Note: λ represents the thermal conductivity at the volumetric water content θ_w, λ_s and λ_d denote the thermal conductivity at saturation and completely dry conditions, θ_s is the volumetric water content at saturation, and θ_{AEV} represents the volumetric water at the AEV.

reduced, i.e., from 1.35 W m^{-1} K^{-1} to 1.01 W m^{-1} K^{-1} (decrease of 25.2%) and 1.59 W m^{-1} K^{-1} to 0.52 W m^{-1} K^{-1} (decrease of 67.3%), as presented in Fig. 14(c) and Fig. 15 (c), respectively. This is owing to the high volumetric water content and low AEV of the WGS and NS, causing sensitivity to the thermal conductivity. In particular, when the GWT level drops from −2 m to −12 m, at the depth of −3 m, the volumetric water content is reduced from 0.5 m^3/m^3 to 0.28 m^3/m^3 for WGS and from 0.35 m^3/m^3 to 0.06 m^3/m^3 for the NS, as shown in Fig. 14(b) and Fig. 15(b), respectively. In contrast, the thermal conductivity of the CLSM is insignificantly affected by the GWT reduction owing to its low volumetric water content and very high AEV. The low volumetric water content in saturation implies a low air content in the dry state. Because the thermal conductivity of air is much lower than that of water [21], a material with a lower volumetric water content has a lower thermal conductivity sensitivity. Furthermore, the AEV of CLSM is 1000 kPa, i.e., 250 times and 166 times higher than that of NS (4 kPa) and WGS (16 kPa), respectively. However, when the GWT level drops from −2 m to −12 m, the maximum suction caused by the decrease in the pore water pressure is 70 kPa (Fig. 16 (a)), which is much lower than that of the AEV of the CLSM. Consequently, the volumetric water content (Fig. 16 (b)) and the thermal conductivity (Fig. 16(c)) of CLSM are not affected by the GWT level drop. The results presented in Fig. 14(c)–Fig. 16(c) can be utilized as input data for heat transfer simulations.

3.4. Heat exchanger performance of HGHEs considering GWT level drop

The thermal conductivity profiles in Fig. 14(c)–Fig. 16(c) were used as the equivalent thermal conductivities in Eq. (4) to study the heat exchanger performance of the HGHEs using COMSOL Multiphysics. Fig. 17 shows the heat exchanger performances of the HGHEs with reference to the decrease in the GWT. It is clear that the heat performances of the HGHEs decrease with a decrease in the GWT, regardless of the backfill material. The HGHE backfilled with NS is the most influenced by the decrease in the GWT. In detail, for the NS, the heat exchange rate at the quasi-steady-state conditions decreases from 968 W to 594 W (63% decrease) when the GWT decreases from −2 to −12 m. This is owing to the high volumetric water content and the low water storage capability (AEV of 6 kPa) of the NS; thus, the drop in the GWT level has the most significant effect on the thermal conductivity of the NS (see Fig. 15). Accordingly, the heat performance of the HGHE backfilled with NS is the most susceptible to the change in the GWT.

Regarding the WGS (Fig. 17(b)) the reduction in the GWT causes a 42% decrease in the heat exchange rate at the quasi-steady-state conditions. Interestingly, when the GWT changes from −2 m to −4 m, the heat exchange rate slightly decreases; however, when the reduction is beyond 2 m, a significant reduction in the heat exchange rate is observed. This result implies that if the change in the GWT causes the suction to exceed the AEV, the water in the largest pore size will be replaced by air leading to a dramatic reduction in the thermal conductivity; consequently, the heat exchange rate of the system will be significantly reduced.

Concerning the CLSM, with the highest AEV and water storage ability, the effect of the GWT level drop is not noticeable. As shown in

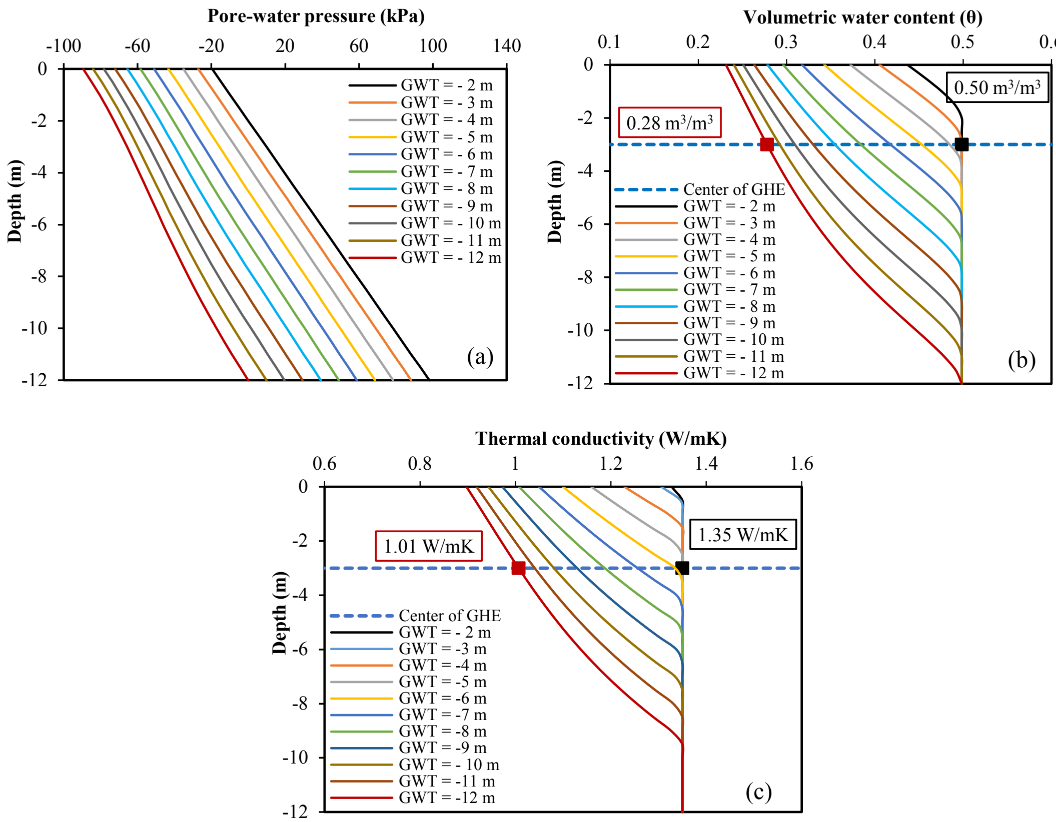

Fig. 14. (a) Pore-water pressure, (b) volumetric water content, (c) thermal conductivity of unsaturated WGS owing to change in groundwater table (GWT).

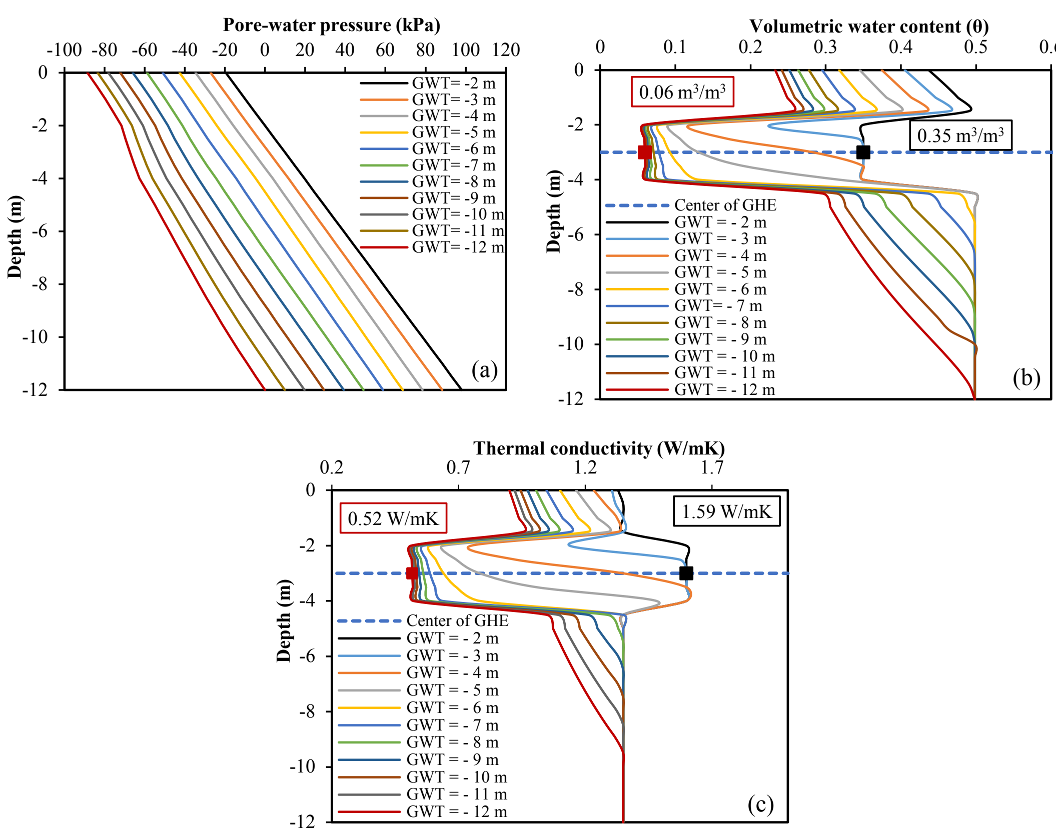

Fig. 15. (a) Pore-water pressure, (b) volumetric water content, (c) thermal conductivity of unsaturated NS owing to change in GWT.

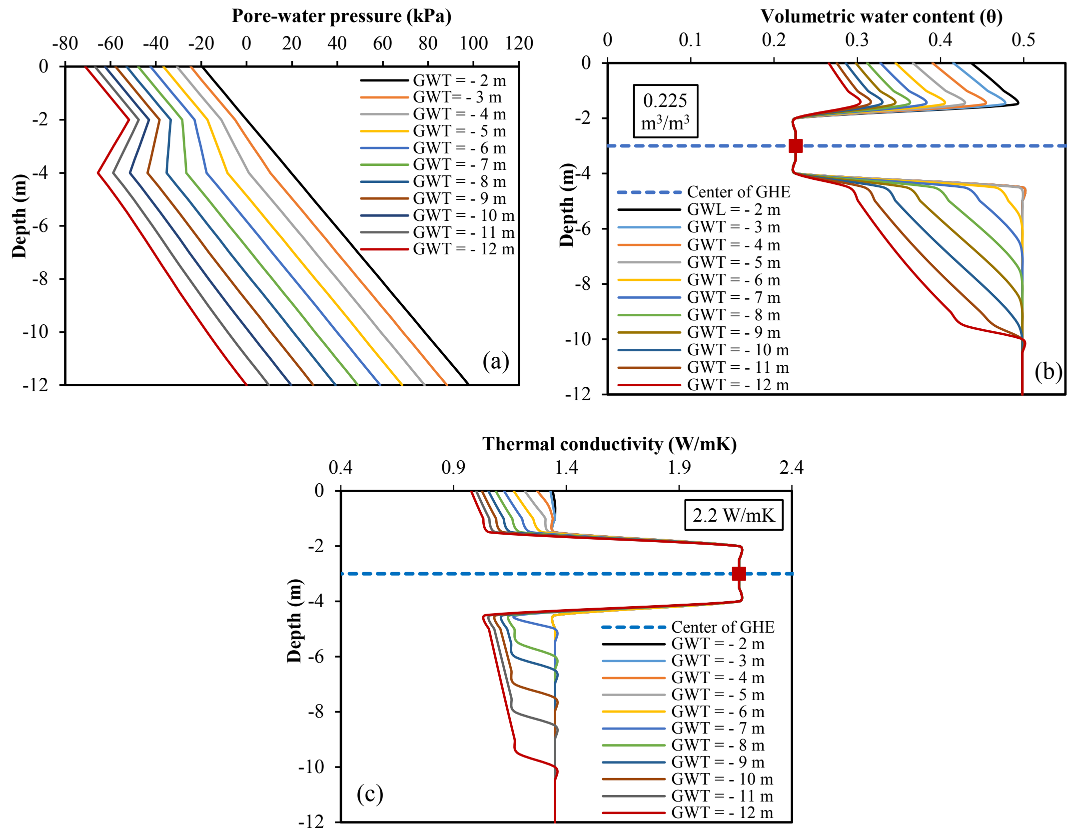

Fig. 16. (a) Pore-water pressure, (b) volumetric water content, (c) thermal conductivity of unsaturated CLSM owing to change in GWT.

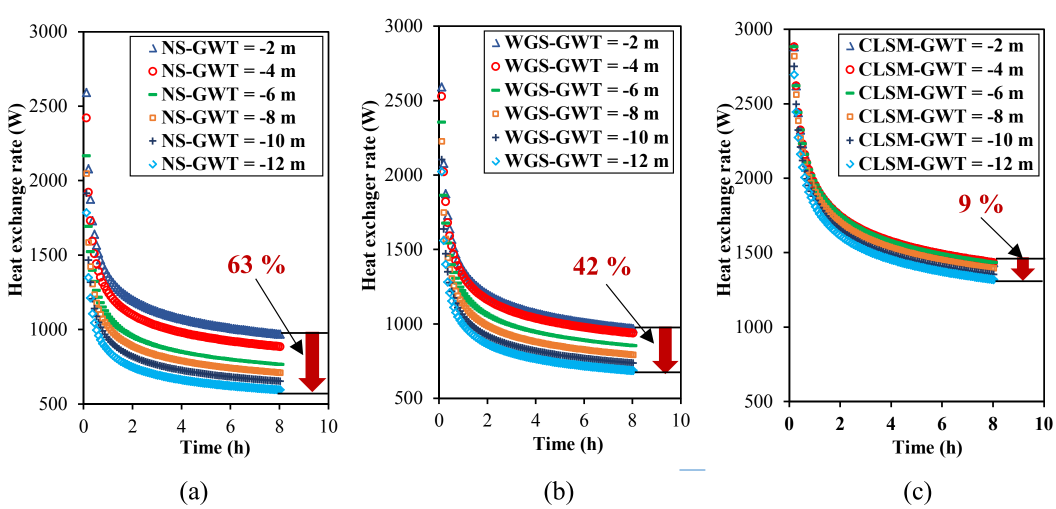

Fig. 17. Heat exchanger performance of HGHEs with (a) NS, (b) WGS, and CLSM.

Fig. 17(c), when the GWT decreases from − 2 m to − 6 m, the heat exchange rate of the system backfilled with CLSM is almost the same as the initial (saturation) condition. However, a slight reduction in the heat exchange rate is observed when the GWT is reduced to −8 m. This is caused by the reduction in the thermal conductivity of the surrounding soil (WGS), and not by the CLSM. As shown in Fig. 18, the thermal conductivity of the CLSM is approximately constant when the GWT level drops from −2 m to −12 m. However, the thermal conductivity of the WGS surrounding the CLSM starts to decrease noticeably when the GWT level drops to −8 m. In detail, at a depth of −5 m, the thermal conductivity at the GWT levels of −8 m and −12 m are 1.17 W m^{-1} K^{-1} and 1.05 W m^{-1} K^{-1}, respectively, i.e., 13.3% and 22.2% lower than those at the GWT level of −4 m (1.35 W m^{-1} K^{-1}), respectively. The results presented above imply that the GWT level drop should be considered when evaluating and designing HGHEs systems to avoid the over-estimations, especially in the areas with a high GWT level drop, or where the soil has a low water storage ability (low AEV) (e.g., sand and sandy soil).

4. Conclusion

This study examined how the GWT level drop influences the heat performance of an HGHE system backfilled with different materials. Based on the results, the following can be drawn:

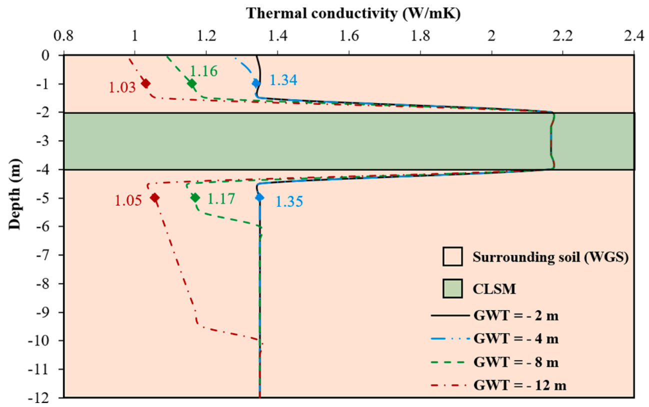

Fig. 18. Thermal conductivity of surrounding soil (WGS) and CLSM at different GWT levels.

1. Thermal conductivities of the WGS, NS, and CLSM under dry conditions are 72.8%, 71.9%, and 47.5% lower than those under saturation, respectively. The CLSM has the lowest difference in the thermal conductivity between saturated and dry conditions owing to its low saturated volumetric water content. This result also demonstrates that the volumetric water content is a significant factor that influencing the thermal conductivity of the backfill materials.
2. The thermal conductivity and volumetric water content can be expressed as a linear relationship, regardless of the backfill material. For the WGS, the thermal conductivity under suction below the AEV is approximately the same as that under the saturation condition.
3. Regarding the WGS and NS, the GWT level drop causes an increase in the suction pressure exceeding the AEV, leading to a reduction in the water content, and a significant reduction in the thermal conductivity. In contrast, the water content and thermal conductivity of the CLSM are negligibly affected by the GWT level drop, as the suction pressure caused by the GWT level drop is significantly lower than the AEV of the CLSM.
4. The heat exchanger performance suggests that a GHE backfilled with NS is most affected by the GWT level drop among the three backfill materials. With regard to the WGS, a noticeable effect only occurs when the change in the GWT causes an increase in the suction that exceeds its AEV. The CLSM has the highest AEV, and thus the heat exchange rate is negligibly reduced when the GWT decreases from −2 m to −6 m. A slight reduction in the heat exchange rate is observed when the GWT level drops to −8 m due to the reduction in the thermal conductivity of the surrounding soil (and not because of the CLSM).
5. GWT reductions should be considered in the design of an HGHE to avoid underestimating the size of the GHE, especially for soils with a low AEV and high reduction in the GWT. As a solution, utilizing backfill materials with low volumetric water contents and low AEVs (such as CLSM) can limit the effect of GWT level drop on the performance of the HGHE.

Declaration of Competing Interest

The authors declare that they have no known competing financial interests or personal relationships that could have appeared to influence the work reported in this paper.

Acknowledgments

This work was supported by the National Research Foundation of Korea (NRF– 2021R1A2B5B01002809) grant funded by the Korean government (MSIT).

References

[1] I.W. Johnston, G.A. Narsilio, S. Colls, Emerging geothermal energy technologies, KSC J. Civil Eng. 15 (4) (2011) 643–653.
[2] A.A. Kojo, J.M. Choi, Current status of the performance of GSHP (ground source heat pump) units in the Republic of Korea, Energy 47 (1) (2012) 77–82, https://doi.org/10.1016/j.energy.2012.05.048.
[3] EPA, A short primer and environmental guidance for geothermal heat pumps. US Environmental Protection Agency; 1997.
[4] E. Kim, J. Lee, Y. Jeong, Y. Hwang, S. Lee, N. Park, Performance evaluation under the actual operating condition of a vertical ground source heat pump system in a school building, Energy Build. 50 (2012) 1–6.
[5] D. D'Agostino, A. Greco, C. Masselli, F. Minichiello, The employment of an earth-to-air heat exchanger as pre-treating unit of an air conditioning system for energy saving: A comparison among different worldwide climatic zones, Energy Build. 229 (2020) 110517, https://doi.org/10.1016/j.enbuild.2020.110517.
[6] H.K. Park, S.R. Lee, S. Yoon, J.C. Choi, Evaluation of thermal response and performance of PHC energy pile: field experiments and numerical simulation, Appl. Energy 103 (2013) 12–24, https://doi.org/10.1016/j.apenergy.2012.10.012.
[7] S. Yoon, S.R. Lee, G.H. Go, A numerical and experimental approach to the estimation of borehole thermal resistance in ground heat exchangers, Energy 71 (2014) 547–555, https://doi.org/10.1016/j.energy.2014.04.104/.
[8] M.J. Kim, S.R. Lee, S. Yoon, G.H. Go, Thermal performance evaluation and parametric study of a horizontal ground heat exchanger, Geothermics 60 (2016) 134–143, https://doi.org/10.1016/j.geothermics.2015.12.009.
[9] G.H. Go, S.R. Lee, N.V. Nikhil, S. Yoon, A new performance evaluation algorithm for horizontal GCHPs (ground coupled heat pump systems) that considers rainfall infiltration, Energy 83 (2015) 766–777, https://doi.org/10.1016/j.energy.2015.02.086.
[10] F. Tang, H. Nowamooz, Outlet temperatures of a slinky-type Horizontal Ground Heat Exchanger with the atmosphere-soil interaction, Renew. Energy 146 (2020) 705–718, https://doi.org/10.1016/j.renene.2019.07.029.
[11] P. Congedo, G. Colangelo, G. Starace, CFD simulations of horizontal ground heat exchangers: a comparison among different configurations, Appl. Therm. Eng. 33–34 (2012) 24–32, https://doi.org/10.1016/j.applthermaleng.2011.09.005.
[12] G. Gan, Dynamic thermal performance of horizontal ground source heat pumps – The impact of coupled heat and moisture transfer, Energy 152 (2018) 877–887, https://doi.org/10.1016/j.energy.2018.04.008.
[13] N.H. Abu-Hamdeh, R.C. Reeder, Soil thermal conductivity: Effects of density, moisture, salt concentration, and organic matter, Soil Sci Soc Am J 64 (4) (2000) 1285–1290.
[14] X. Xua, W. Zhanga, C. Fana, G. Lia, Effects of temperature, dry density and water content on the thermal conductivity of Genhe silty clay, Results Phys. 16 (2020), 102830.
[15] M. Allan, S. Kavanaugh, Thermal conductivity of cementitious grouts and impact on heat exchanger length design for ground source heat pumps, HVAC R Res. 5 (2) (1999) 85–96, https://doi.org/10.1080/10789669.1999.10391226.
[16] F. Delaleux, X. Py, R. Olives, A. Dominguez, Enhancement of geothermal borehole heat exchangers performances by improvement of bentonite grouts conductivity, Appl. Therm. Eng. 33-34 (2012) 92–99, https://doi.org/10.1016/j.applthermaleng.2011.09.017.
[17] A.A. DiCarlo, C.E. Videchak, R.A. Caldwell, Optimization of Spatially Distributed Soil Conductivities for Horizontal Ground Heat Exchangers, Appl. Therm. Eng. 167 (2020) 114793, https://doi.org/10.1016/j.applthermaleng.2019.114793.
[18] H.M. Choi, J.Y. Lee, Changes of groundwater conditions on Jeju volcanic island, Korea: implications for sustainable agriculture, Afr. J. Agric. Res. 7 (4) (2012) 647–661.
[19] J. Kim, J. Lee, M. Petitta, H. Kim, D. Kaown, I.-W. Park, S. Lee, K.-K. Lee, Groundwater system responses to the 2016 ML 5.8 Gyeongju earthquake, South Korea, J. Hydrol. 576 (2019) 150–163, https://doi.org/10.1016/j.jhydrol.2019.06.044.
[20] B. Lee, S.Y. Hamm, S. Jang, J.Y. Cheong, G.-B. Kim, Relationship between groundwater and climate change in South Korea, Geosci. J. 18 (2) (2013) 209–218, https://doi.org/10.1007/s12303-013-0062-7.
[21] B.H. Dinh, Y.-S. Kim, G.-o. Kang, Thermal conductivity of steelmaking slag-based controlled low-strength materials over entire range of degree of saturation: A study for ground source heat pump systems, Geothermics 88 (2020) 101910, https://doi.org/10.1016/j.geothermics.2020.101910.
[22] Y.S. Kim, H.B. Dinh, M.T. Do, G.O. Kang, Development of thermally enhanced controlled low-strength material incorporating different types of steel-making slag for ground-source heat pump system, Renew. Energy 150 (2020) 116–127, https://doi.org/10.1016/j.renene.2019.12.129.
[23] A.C.I. Committee, 229R, Controlled Low Strength Materials (ACI 229R–99), American Concrete Institute, Farmington Gill, MI, USA, 1999.
[24] Y.-S. Kim, T.M. Do, M.-J. Kim, B.-J. Kim, H.-K. Kim, Utilization of by-product in controlled low-strength material for geothermal systems: engineering performances, environmental impact, and cost analysis, J. Clean. Prod. 172 (2018) 909–920.
[25] D.G. Fredlund, A. Xing, Equations for the soil-water characteristic curve, Can. Geotech. J. 31 (4) (1994) 521–532, https://doi.org/10.1139/t94-06.
[26] S.W. Churchill, Friction factor equations span all fluid-flow regimes, Chem. Eng. 84 (24) (1997) 91.
[27] ASTM D5334, Standard test method for determination of thermal conductivity of soil and soft rock by thermal needle probe procedure, 2004.

[28] D.A. De Vries, Thermal properties of soils, in: W.R. Van Wijk, (Ed.), Physics of Plant Environment, North-Holland, Amsterdam, 1963, pp. 210-235.
[29] S. Naylor, S.M. Kevin, M. Ellett, A.R. Gustin, Spatiotemporal variability of ground thermal properties in glacial sediments and implications for horizontal ground heat exchanger design, Renew. Energy 81 (2015) 21–30.
[30] D.H. Kim, G.M. Kim, H.J. Baek, Relationship between thermal conductivity and soil–water characteristic curve of pure bentonite-based grout, Int. J. Heat Mass Transfer 84 (2015) 1049–1055, https://doi.org/10.1016/j.ijheatmasstransfer.2015.01.091.